Functional Groups and Sulfur K-Edge XANES Spectra: Divalent Sulfur and Disulfides

Ana Mijovilovich,*,†,‡ Lars G. M. Pettersson,§ Frank M. F. de Groot,† and Bert M. Weckhuysen*,†

Inorganic Chemistry and Catalysis group, Department of Chemistry, Utrecht University, Sorbonnelaan 16, 3584 CA, Utrecht, The Netherlands, and Department of Physics, Alba Nova, Stockholm University, SE 106 9 L Stockholm, Sweden

Sulfur K-edge XANES was measured for two divalent sulfurs (dibenzyl and benzyl phenyl) and two disulfides (dibenzyl and diphenyl). The absorption spectra could be assigned using density functional theory with the "half core hole" approximation for the core hole including relaxation of selected excited states at the absorption edge. Analysis of the molecular orbitals shows that the characteristic double peak of the dibenzyl disulfide arises as a consequence of the enhanced splitting of the LUMO (lowest unoccupied molecular orbital) and the LUMO + 1. Exchange of the ligand benzyl by phenyl introduces more transitions at the absorption edge, which enhance the broadening in the divalent sulfur and splitting of the peaks of the disulfide. It is shown that different ligand groups introduce significant differences in the absorption edge, which poses a problem for the speciation analysis when the ligand groups are not clearly defined.

1. Introduction

Sulfur K-edge XANES (X-ray absorption near edge structure) is used for speciation of sulfur compounds in diverse fields, such as biology,[1–5] geology,[6] archeology,[7] diesel car emissions,[8] and oil and coal studies.[9–13] These studies rely upon the assumption that there is a small set of significant and different components that model the samples. Usually one member of a class (such as thiols, sulfides, sulfones, etc.) is used for speciation, irrespective of the identity of the ligands to the sulfur. For example, the differences between thiol and disulfide allowed Rompel et al.[4] to determine the redox status in blood, plasma, and erythrocytes. In that work, reduced glutathione resembles cysteine, whereas oxidized glutathione resembles cystine. Sarangi et al.[14] showed that identical functional groups can give different S K-edge XANES, for example, for cystine and 3-methylpropylene disulfide, among others. The independence and diversity of the components will have an impact on the accuracy of the composition analysis. In order to build the most appropriate database of compounds, a more fundamental understanding of the XANES, relating the transitions to molecular orbitals and geometric and symmetry properties of the compounds, is highly needed. Special attention should be given to avoid experimental errors (self-absorption in fluorescence detection, or uneven surfaces in electron detection), which have been reviewed in detail in the literature.[15,16]

Density functional theory (DFT) calculations exist in the literature for sulfur compounds of different chemical nature (inorganic, amino acids, and aromatic).[14,17–20] In the above-mentioned work, Sarangi et al.[14] used TD-DFT to simulate the XAS spectra. Damian-Risberg et al.[19] have explained how the XANES structures are affected by the differences in protonation in cysteine and cystine solutions at different pH values using

the StoBe-deMon code.[21] Also the XANES spectra of inorganic compounds (sulfur dioxide, sulfite, and sulfonate solutions and of the substituted sulfonate ions $X_3C_8O_3^-$ with X = H, Cl, F) have been analyzed with DFT.[17] For the heterocyclic compounds that are relevant in oil and coal there is, however, no systematic study of the geometric and electronic structure determinants of the XANES.[9]

In a recent publication[20] we have studied with DFT two thiophenes (dibenzothiophene and dibenzothiophene sulfone) and DL-methionine, and shown the differences introduced by the sulfone on the dibenzothiophene. Both dibenzothiophene and DL-Methionine show a similar white line. The similar edge position prevents the use of the energy of the edge for component analysis. We have shown that the differences in the width of the white line are due to the different intensity ratio for the three transitions at the edge. High-resolution measurements and a careful analysis of the white line widths could thus provide additional information for the XANES component analysis.

No theoretical works exist about the XANES of dibenzyls. The chemical interest is on exploring the possibility to speciate sulfide from disulfide. From the theory point of view it is interesting to study the "determinants of the XANES" by studying the changes induced by a different ligand, without a significant change in the symmetry or the formal valence at the sulfur. This points to the problem of determining "categories" of compounds in sulfur compound speciation. Sulfur XANES shows a characteristic broad oscillation after the edge that causes uncertainties in the background determination. We have analyzed where the Rydberg states seem to start being important, giving rise to this broad oscillation after the edge.

In this paper we report the XANES experiments and DFT simulations for dibenzyl sulfide ($C_{14}H_{14}S$) and dibenzyl disulfide ($C_{14}H_{14}S_2$) (see Figure 1). The effect on the electronic structure of the compound by exchanging ligands is studied in the benzyl phenyl sulfide ($C_{13}H_{12}S$) and diphenyl disulfide ($C_{12}H_{10}S_2$). The character of the lowest unoccupied molecular orbitals (LUMOs), corresponding to the first transitions is analyzed. We show how

* To whom correspondence should be addressed. E-mail: Ana.Mijovilovich@lightsource.ca and b.m.weckhuysen@uu.nl.
† Utrecht University.
‡ Present address: The Canadian Light Source Inc., University of Saskatchewan, 101 Perimeter Road, Saskatoon, SK, S7N 0X4, Canada.
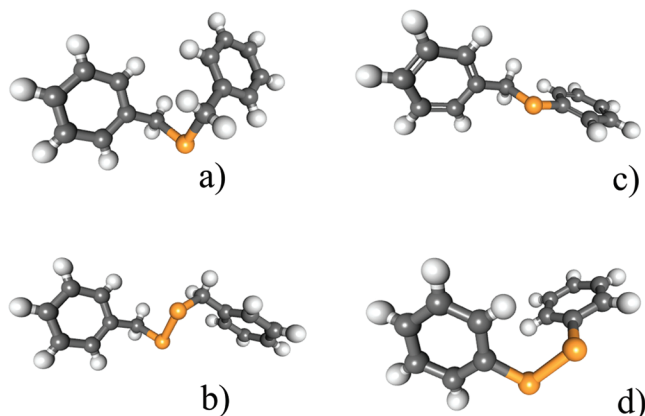§ Stockholm University.

Figure 1. Molecular structure of: (a) dibenzyl sulfide (zzzsry01.pdb), (b) dibenzyl disulfide (benzss05.pdb). (c) benzyl phenyl sulfide (www.chemspider.com, ID 12697.mol) and (d) diphenyl disulfide (phess01.pdb).

the S−S bond affects the shape and intensity of the first resonance and how significant the changes are in the XANES induced by the exchange of benzyl by phenyl.

2. Materials and Methods

Dibenzyl sulfide, benzyl phenyl sulfide, diphenyl disulfide, and dibenzyl disulfide were purchased from Sigma Aldrich (98% pure). The X-ray microscopy beamline ID21 in ESRF (unfocused) was used for collecting sulfur K-edge XANES.[22] The beamline has a Si(111) monochromator for selecting the energies. Fluorescence was collected with a Ge detector. The energy scale was calibrated using gypsum, assigning a value of 2482.90 eV to the maximum of the first resonance (white line). Sample fine powder was spread on sulfur-free polyimide tape and measurements were performed in vacuum, on 4 homogeneous spots on the sample selected using the in situ microscope.

An energy range of −100 eV to +400 eV with respect to the edge position was used for the data. The package ATHENA[23−25] was used for the data reduction, using the Autobackup routine[26] for the background reduction, and also for calculating the area of the white line, by fitting an arctangent and a Gaussian, with centers (fixed) at the maximum of the first derivative and at the maximum point of the edge, respectively.

The code StoBe-deMon[21] was used for the DFT simulations. The nonlocal exchange functional from Perdew and Wang[27] and the correlation functional from Perdew[28,29] were used. Half of an electron was removed from the 1s to generate the potential (half core hole, abbreviated as HCH)[30] used to determine all excited states.

The basis sets used were: (621/41/1) for C and (311/1) for H. The auxiliary basis sets (N^C-s, N^C-spd; N^{XC}-s, N^{XC}-spd) were used to fit the density in the Coulomb interaction, and to interpolate the exchange-correlation potential over the numerical grid they were (5, 4; 5, 4) for S, (5, 2; 5, 2) for C, and (3, 1; 3, 1) for H. The IGLO III basis[31] was used for the sulfur. For disulfides the core hole was localized on the absorber sulfur, with the other sulfur as spectator. Using a bigger basis set, (6311/311/1), for C in the core hole localized model did not significantly affect the results. The spectra for benzyl phenyl sulfide shown in the paper are with the bigger basis, and the ionicity and DOS are shown in the smaller basis to compare with the other compounds.

A double basis set approach is used in which the excited states are obtained from a single diagonalization of the Kohn−Sham matrix constructed using the converged HCH density with a large set of diffuse basis functions added. The dipole transition elements between the initial and final states were calculated. In the HCH method of Triguero et al.[30] both initial and final states are described with the same set of molecular orbitals.

The spectra were calibrated in energy by calculating the lowest core-excited state in the presence of a single hole in the 1s level.[32] The energy was shifted by +7.4 eV to account for the relativistic correction.[17] An additional ad hoc shift of −0.3 eV was needed for calibrating the spectra, in agreement with the results of Damian-Risberg et al.[17] for sulfides. In the case of the disulfides the correction was −2.45 eV.

The spectra were generated by convoluting the discrete spectral transitions with Gaussian functions.[17] Gaussians were used instead of the theoretical Voigt line, since no parameters are available to build the profile, and further broadening effects occur in solid samples (excitation of phonons, band structure effects, screening, local disorder, etc). Below the ionization potential the full width at half-maximum (fwhm) of the Gaussian was chosen to match the experimental broadening in a generic beamline using a Si(111) monochromator. This means a starting fwhm of 0.5 eV. The fwhm was linearly increased to 4 eV over a range of 20 eV and then kept constant, simulating the approach toward the continuum. The maximum broadening of 4 eV gave good agreement with experiment as in Mijovilovich et al.[20]

The Löwdin densities of states (DOS) were calculated for the alpha spins for the unoccupied states for the HCH approximation and the lowest unoccupied molecular orbitals (LUMO) were plotted with MOLEKEL.[33]

3. Results

3.1. Experimental Results. Figure 2 shows the experimental XANES spectra of two sulfides (dibenzyl and benzyl phenyl) and two disulfides (dibenzyl and diphenyl). (Notice that a real sulfide is a dianionic mononuclear S and not an sp^3 hybridized divalent covalent S. The term "sulfide" will still be used throughout for reasons of simplicity.)

The dibenzyl sulfide shows a strong white line, and the edge position (at 2473.5 eV) is in agreement with previous literature.[10] The disulfide compound shows a decreased intensity and more structure at the white line than the sulfide. The decrease in the white line intensity is about one-third with respect to the dibenzyl sulfide. An after-edge range of 110 eV was needed for the background subtraction in order to avoid misleading effects from the long oscillations after the edge that are typical of sulfur K-edges. Calculating the area change by fitting an arctangent and a Gaussian, shows that the decrease of the intensity and the enhancement of the white line width for the disulfide imply an area decrease of about 40% compared to the sulfide. The position of the edge for disulfide is shifted to lower energy by 0.5 eV with respect to the sulfide, as measured from the top of the white line.

The exchange of the benzyl by a phenyl ligand causes significant changes in the white line of the spectra for both sulfide and disulfide. In the case of the benzyl phenyl sulfide the white line is broader with a reduced intensity compared to the dibenzyl compound, whereas for the disulfide the two peaks at the edge are broader and have a wider separation, suggesting that more than one transition might be present. The edge position is slightly affected by the benzyl ligand in the sulfide compound only (at 2474.3 eV), while the diphenyl disulfide has the edge at about 2472.9 eV, similar to the dibenzyl disulfide.
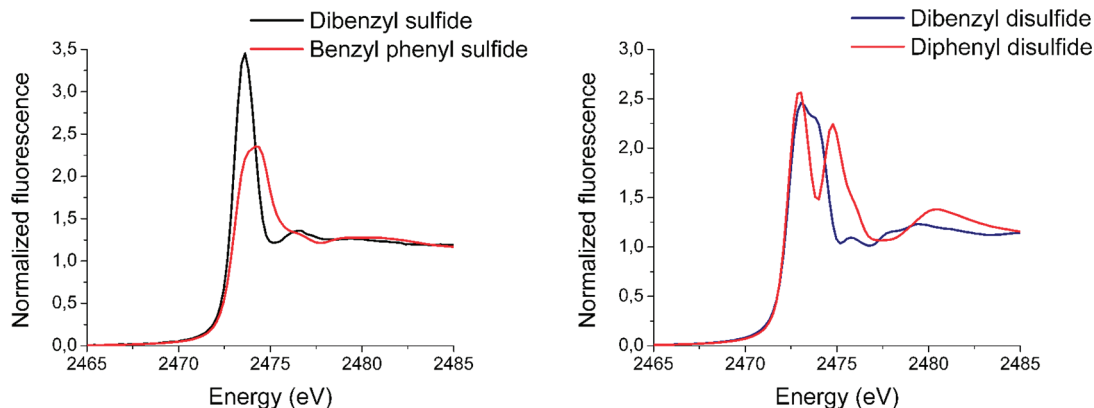
Functional Groups and Sulfur K-Edge XANES Spectra

J. Phys. Chem. A, Vol. 114, No. 35, 2010 **9525**

Figure 2. Experimental XANES spectra for: sulfides (left) and disulfides (right).

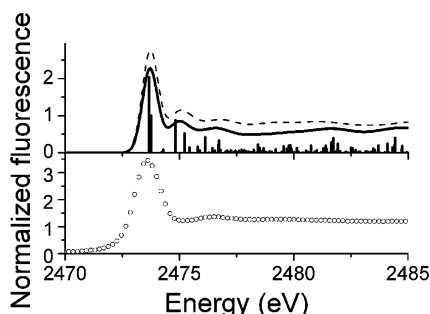**Figure 3.** Simulations for dibenzyl sulfide. From bottom to top: (a) experiment, (b) HCH with the transitions (drop lines) and the Löwdin DOS (dashed line).
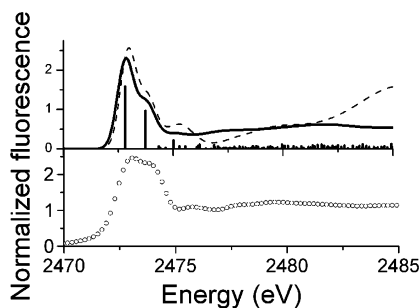

Figure 5. Simulations for benzyl phenyl sulfide. From bottom to top: (a) experiment, (b) HCH with the transitions (drop lines) and the Löwdin DOS (dash line).

Figure 4. Simulations for dibenzyl disulfide. From bottom to top: (a) experiment, (b) HCH with the transitions (drop lines) and the Löwdin DOS (dash line).

Figure 6. Simulations for diphenyl disulfide. From bottom to top: (a) experiment, (b) HCH with the transitions (drop lines) and the Löwdin DOS (dash line).

3.2. Simulations with StoBe. *3.2.a. Dibenzyl Sulfide.* In Figure 3 the experimental XANES of dibenzyl sulfide is shown at the bottom, and the stacked spectra show the HCH with the corresponding transition lines and the HCH DOS densities. A good agreement with the experiment is obtained with the HCH model. The simulation gives all the features after the edge, though shifted in energy due to the lack of relaxation of the excited states in this calculation.

The HCH DOS is similar to the HCH where matrix elements are included, implying that in this case the effects of including the computed transition-dipole matrix elements is small; the transitions are thus in this case well-described by the unoccupied density of states from the HCH calculation.

3.2.b. Dibenzyl Disulfide. The calculated spectra together with the experiment of dibenzyl disulfide are shown in Figure 4. Again, the HCH proves to be a good model for the sulfur XANES. The double peak of the white line is nicely reproduced, although a linear broadening is not enough to match the intensity of the second peak in the white line. As was also the case for
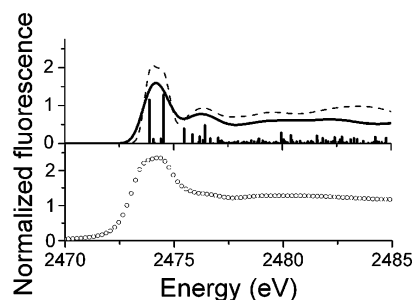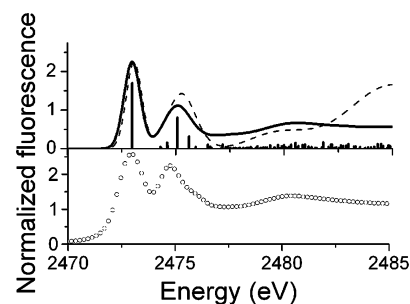
dibenzyl sulfide, the HCH DOS is similar to the calculated HCH XANES spectrum.

3.2.c. Benzyl Phenyl Sulfide. The simulated spectra together with the experiment for benzyl phenyl sulfide are presented in Figure 5. The HCH gives a fair reproduction of all features in the experiment. However, the oscillations after the edge are too dominant. The white line is composed of six transitions with two most intense lines (LUMO and LUMO + 5). The HCH DOS shows some differences with the HCH due to the matrix element in the total cross section of the transition.

3.2.d. Diphenyl Disulfide. Figure 6 shows the simulated and experimental XANES spectra of diphenyl disulfide. The HCH simulation gives a quite reasonable representation of the spectrum. In the experiment the energy separation between the two peaks of the edge in diphenyl disulfide is higher than for dibenzyl disulfide. This is explained as due to the presence of additional molecular orbitals in the case of phenyl ligands, with the intense transition (with most of the electron density at the sulfur) at higher energy.
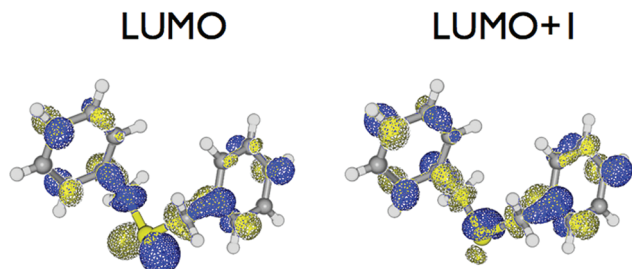
Figure 7. Lowest core-excited states: LUMO (left) and LUMO + 1 (right), for dibenzyl sulfide.
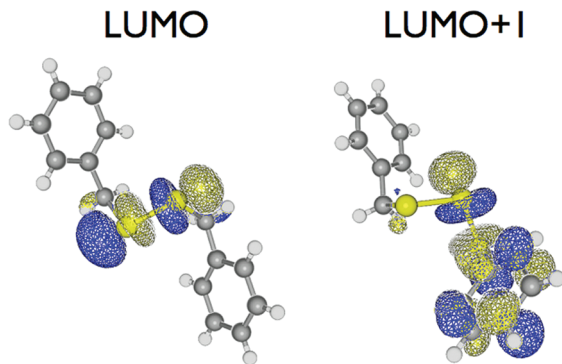

Figure 8. Core-excited states, LUMO (left) and LUMO + 1 (right), for dibenzyl disulfide.

3.3. Analysis of the Molecular Orbitals. *3.3.a. Dibenzyl Sulfide.* In Figure 7 the LUMO and LUMO + 1 for the HCH model corresponding to the two transitions composing the white line, are shown. The LUMO has a predominant σ^*(S−C) character and the LUMO + 1 has π^*(S−C) character. That is, the LUMO + 1 orbital at the sulfur is rotated 90° with respect to the LUMO.

3.3.b. Dibenzyl Disulfide. The molecular orbitals corresponding to the transitions compounding the white line for the HCH model, the LUMO, and LUMO + 1, are shown in Figure 8. The LUMO shows σ^*(S−S) character. In the LUMO + 1 the absorbing sulfur has much lower amplitude than the spectator sulfur. The contribution to the transition from the antibonding π^* S−S bond is surpassed by the contribution from the S−C bond with σ^* character.

3.3.c. Benzyl Phenyl Sulfide. In Figure 9 the MOs corresponding to the first 6 transitions are shown. The LUMO shows that most of the electron density for the ligand is mostly at the benzyl with π_u orbital. The bond S−C(benzyl) shows a σ_u orbital at the LUMO, and at the sulfur a hybrid of s+p_z. The other intense transition (6th) shows a π orbital at the sulfur. The transitions 2 and 3 have most of the electron density at the phenyl ligand and mostly in σ_u orbitals, while transitions 4 and 5 have most of the electron density at the phenyl involving a π^*_g orbital. It is interesting to note that the MOs at the sulfur for the most intense transitions (first and sixth) are similar to the MOs at the dibenzyl sulfide in reverse order (second and first).

3.3.d. Diphenyl Disulfide. The first, sixth, and seventh transitions are the most intense, giving rise to the two peaks at the white line. The MOs for the most intense transitions in the white line can be seen in Figure 10. The LUMO at the sulfur is very similar to the LUMO in dibenzyl disulfide. The same happens with the LUMO + 5 at the sulfur for both compounds. The LUMO + 1 and LUMO + 2 are degenerate with σ and π MOs respectively. The LUMO + 3 and LUMO + 4 are also

degenerate with most of the electron density in one phenyl in a combination of π (bonding and antibonding) orbitals.

4. Discussion

4.1. Sulfur K-Edge Spectra and Their DFT Simulations. The experimental results for dibenzyl sulfide are in agreement with Waldo et al.[10] and also the sulfide compound from Grossman et al.,[34,35] whereas the sulfide compound measured by Kelemen et al.[36] shows a less intense white line, maybe due to self-absorption. The enhancement of the area of the white line for the disulfide with respect to sulfide indicates changes in the molecular orbital structure. The rather small shift of 0.28 eV in the edge position of the disulfide to lower energy suggests that changes in the effective nuclear charge of the sulfur due to a sulfur instead of the organic ligand are minimal. The little difference found in the calculated ionicities of the dibenzyls (0.248 and 0.177 for sulfide and disulfide, respectively) confirms this hypothesis. The higher ionicity for the sulfide compared to the disulfide is in agreement with the observed shift to lower energy of the disulfide absorption edge, and gives strong indications that the change in the effective nuclear charge is the main reason for the edge shift.

In the case of the benzyl phenyl sulfide the edge is at slightly higher energy than in the dibenzyl sulfide. The slightly higher ionicity value (0.264) is in agreement with this result.

The exchange of benzyl by phenyl breaks the symmetry of the molecule, and this is reflected in the electron density distribution. In the case of the benzyl phenyl sulfide most of the electron density is on the benzyl ligand and the S−C bond to the benzyl, whereas in dibenzyl sulfide the electron densities are similar for both ligands.

4.2. Determinants of the XANES. In dibenzyl sulfide, the LUMO has mainly σ^* (S−C) character whereas the LUMO + 1 has mainly π^*(S−C) character. This is in agreement with the assignments of Dezarmaud-Dandine et al.[37] and Sarangi et al.[38]

In dibenzyl disulfide the assignment of the LUMO to a molecular orbital with σ^*(S−S) character is in agreement with the results of Hitchcock et al.[18] for dimethyl sulfide and Damian-Risberg et al.[17] for cystine in solution at pH 7.1. The characteristic structure at the white line of the disulfides emerges as a consequence of the splitting between LUMO and LUMO + 1 being bigger than in the sulfides. Sarangi et al.[14] find in cystine a LUMO + 1 composed of an antibonding σ^*(S−C) and π^*(S−S), using a TDDFT calculation of the XAS. Damian-Risberg et al.[17] find the same σ^* (S−C) predominant character for the higher LUMOs composing the second peak of the white line. The dibenzyl disulfide results of this work are in general agreement with published results on cystine, with the most important contribution to the LUMO + 1 transition from the S−C bond with σ^* character (similar to the LUMO in dibenzyl sulfide), and also some contribution from the antibonding π^* from the S−S bond. In contrast to the case of cystine,[14,19] for dibenzyl disulfide there are no degenerate states contributing to the white line.

The addition of new transitions at the lowest LUMOs makes the white line broader in the case of benzyl phenyl sulfide, while the diphenyl disulfide shows the splitting of the edge characteristic of disulfides, but broader than in dibenzyls, due to the additional transitions introduced by the phenyl ligand.

4.3. Borderline of Valence and Rydberg States. The higher intensity of the white line in the dibenzyl sulfide is due to the two very close, high intensity transitions, while the benzyl phenyl sulfide has more transitions that are more spread out, giving rise to a broader, lower intensity white line. Close after
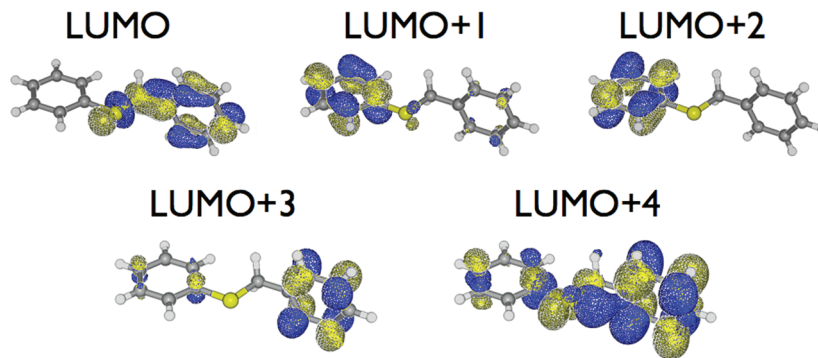
LUMO   **LUMO+1**   **LUMO+2**

LUMO+3   **LUMO+4**

Figure 9. Core-excited states, first five LUMOs, of benzyl phenyl sulfide.

LUMO   **LUMO+1**   **LUMO+2**
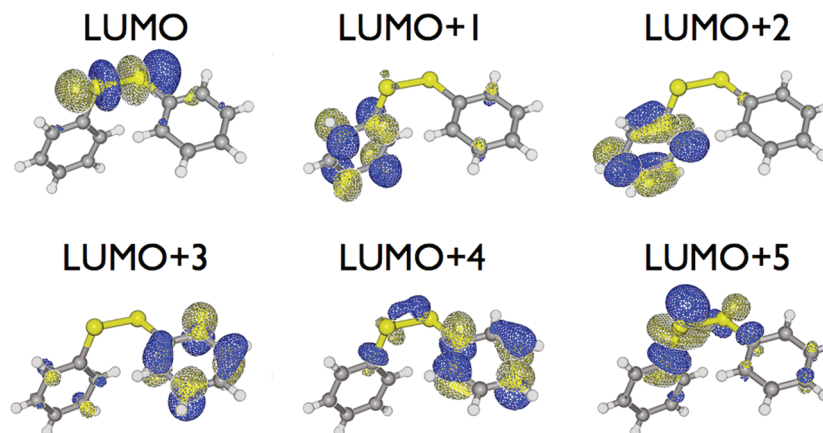
LUMO+3   **LUMO+4**   **LUMO+5**

Figure 10. Core excited states, first six LUMOs, of diphenyl disulfide.

the white line the density of transitions increases, which indicates that the Rydberg states dominate this region. The area of the spectrum dominated by valence character seems to be reduced to the absorption edge only. In a former work[20] we showed that only for Dibenzothiophene, where the Rydberg states are rather separated in energy from the first LUMOs, variational relaxation[32] of the first 15 transitions could be included and significantly improved the simulation. At this point the molecular orbital interpretation of XANES can be synchronized with the real space full multiple-scattering theory (FEFF8),[39,40] by considering the diffuse Rydberg orbitals as the MO representation of the (space spread) diffracted photoelectron wave function.

5. Conclusions

The sulfur−sulfur bonding introduces a large change in the shape and intensity of the white line due to the enhanced splitting between LUMO and LUMO + 1 in disulfide compared to the sulfide. Similar disulfide groups can show similar XANES, as is the case of dibenzyls and cystine with a double peak white line. However, considering in detail the electronic structure, small differences appear, with two transitions contributing to the white line in dibenzyl disulfide and four transitions for cystine.[19] These additional transitions in cystine are either degenerate or of low intensity. Different binding ligands introduce differences in the shape of the white line as well as shifts in the edge position. The origin can be traced to the changes in the MOs arising from the different group symmetry (monoclinic for dibenzyl disulfide and hexagonal in cystine).

The bound states dominate the spectra at the edge and including the full relaxation of these transitions give an improvement of the edge simulation; the proximity of the Rydberg states to the white line in the case of both disulfides makes this correction to the individual line positions uncertain for more than the lowest states at the edge, however.

For the speciation of sulfides and disulfides, the differences in edge position and white line intensities can be used for component analysis. The XANES edge is not indifferent to specific binding groups, and this poses a problem in cases where coordination to different groups is possible. In a mixture with other sulfur compounds, where separation of disulfide from sulfide would be difficult, an enhanced white line width is an indicator of the simultaneous presence of disulfides and sulfides. Sulfur speciation using XANES provides a unique level of detail at the molecular and electronic structure level in the analysis of crude oil components. The XANES technique could be used to enhance the prediction capabilities of a recently proposed method to predict a large range of physicochemical properties of crude oil and bitumen mixtures using either IR spectra or a combination of IR and NMR spectra.[41−43]

Supporting Information Available: Structure files corresponding to each panel in Figure 1 are provided. Panel: a (jp103109y_si_004.cif), b (jp103109y_si_003.cif), c (jp103109y_si_003.mol, Jmol file; also www.chemspider.com, ID 12697),

d (jp103109y_si_005.cif). This material is available free of charge via the Internet at http://pubs.acs.org.

References and Notes

(1) Pickering, I. J.; Prince, R. C.; Divers, T.; George, G. N. *FEBS Lett.* **1998**, *441*, 11.

(2) Prange, A.; Dahl, C.; Trüper, H. G.; Behnke, M.; Hahn, J.; Modrow, H.; Hormes, J. *Eur. Phys. J., D* **2002**, *20*, 589.

(3) Dauphin, Y.; Cuif, J. P.; Salomé, M.; Susini, J. *Am. Mineral.* **2005**, *90*, 1748.

(4) Rompel, A.; Cinco, R. M.; Latimer, M. J.; McDermott, A. E.; Guiles, R. D.; Quintanlha, A.; Krauss, R. M.; Sauer, K.; Yachandra, V. K.; Klein, M. P. *Proc. Natl. Acad. Sci. U.S.A.* **1998**, *95*, 6122.

(5) Hedman, B.; Frank, P.; Penner-Hahn, J. E.; Roe, A. L.; Hodgson, K. O.; Carlson, R. M. K.; Brown, G.; Cerino, J.; Hettel, R.; Troxel, T.; Winick, H.; Yang, J. *Nucl. Instrum. Methods Phys. Res., Sect. A* **1986**, *246*, 797.

(6) Majzlan, J.; Myneni, S. C. B. *Environ. Sci. Technol.* **2005**, *39*, 188.

(7) Sandström, M.; Jalilehvand, F.; Persson, I.; Gelius, U.; Frank, P.; Hall-Roth, I. *Nature* **2002**, *415*, 893.

(8) Matsumoto, S.; Tanaka, Y.; Ishii, H.; Tanabe, T.; Kitajima, Y.; Kawai, J. *Spectrochim. Acta, Part B* **2006**, *61*, 991.

(9) George, G. N.; Gorbaty, M. L. *J. Am. Chem. Soc.* **1989**, *111*, 3182.

(10) Waldo, G. S.; Mullins, O. C.; Penner-Hahn, J. E.; Cramer, S. P. *Fuel* **1992**, *71*, 53.

(11) Sarret, G.; Connan, J.; Kasrai, M.; Bancroft, G. M.; Charriè-Duhaut, A.; Lemoine, S.; Adam, P.; Albrecht, P.; Eybert-Bèrard, L. *Geochim. Cosmochim. Acta* **1999**, *63*, 3767.

(12) Huffman, G. P.; Mitra, S.; Huggins, F. E.; Shah, N.; Vaidya, S.; Lu, F. *Energy Fuels* **1991**, *5*, 574.

(13) Kasrai, M.; Bancroft, G. M.; Brunner, R. W.; Jonasson, R. G.; Brown, J. R.; Tan, K. H.; Feng, X. *Geochim. Cosmochim. Acta* **1994**, *58*, 2865.

(14) Sarangi, R.; Frank, P.; Hodgson, K. O.; Hedman, B. *Inorg. Chim. Acta* **2008**, *361*, 956.

(15) Solomon, E. I.; Hedman, B.; Hodgson, K. O.; Dey, A.; Szilagyi, R. K. *Coord. Chem. Rev.* **2005**, *249*, 97.

(16) George, G. N.; Gnida, M.; Bazylinski, D. A.; Prince, R. C.; Pickering, I. J. *J. Bacteriol.* **2008**, *190*, 6376.

(17) Damian-Risberg, E.; Eriksson, L.; Mink, J.; Pettersson, L. G. M.; Skripkin, M. Y.; Sandström, M. *Inorg. Chem.* **2007**, *46*, 8332.

(18) Hitchcock, A. P.; Bodeur, S.; Tronc, M. *Phys.B* **1989**, *158*, 257.

(19) Risberg, E. D.; Jalilehvand, F.; Leung, B. O.; Pettersson, L. G. M.; Sandström, M. *Dalton Trans.* **2009**, 3542.

(20) Mijovilovich, A.; Pettersson, L. G. M.; Mangold, S.; Janousch, M.; Susini, J.; Salomé, M.; De Groot, F. M. F.; Weckhuysen, B. M. *J. Phys. Chem. A* **2009**, *113*, 2750.

(21) Hermann, K.; Pettersson, L. G. M.; Casida, M. E.; Daul, C.; Goursot, A.; Koester, A.; Proynov, E.; St-Amant, A.; Salahub, D. R.; Carravetta, V.; Duarte, H.; Godbout, N.; Guan, J.; Jamorski, C.; Leboeuf, M.; Malkin, V.; Malkina, O.; Nyberg, M.; Pedocchi, L.; Sim, F.; Triguero, L.; Vela, A. *StoBe-deMon Code;* 2001.

(22) Susini, J.; Salomé, M.; Fayard, B.; Ortega, R.; Kaulich, B. *Surf. Rev. Lett.* **2002**, *9*, 203.

(23) Ravel, B. http://cars9.uchicago.edu/~ravel/software/exafs/, 2005.

(24) Ravel, B.; Newville, M. *J. Synchrotron Radiat.* **2005**, *12*, 537.

(25) Newville, M. *J. Synchrotron Radiat.* **2001**, *8*, 322.

(26) Newville, M.; Livins, P.; Yacoby, Y.; Rehr, J. J.; Stern, E. A. *Phys. Rev. B* **1993**, *47*, 14126.

(27) Perdew, J. P.; Wang, Y. *Phys. Rev. B* **1986**, *33*, 8800.

(28) Perdew, J. P. *Phys. Rev. B* **1986**, *33*, 8822.

(29) Perdew, J. P. *Phys. Rev. B* **1986**, *34*, 7406.

(30) Triguero, L.; Pettersson, L. G. M.; Ågren, H. *Phys. Rev. B* **1998**, *58*, 8097.

(31) Kutzelnigg, W.; Fleischer, U.; Schindler, M. *NMR—Basic Principles and Progress*; Springer: Berlin, Heidelberg, NewYork, 1990.

(32) Kolczewski, C.; Puttner, R.; Plashkevych, O.; Ågren, H.; Staemmler, V.; Martins, M.; Snell, G.; Schlachter, A. S.; Sant'Anna, M.; Kaindl, G.; Pettersson, L. G. M. *J. Chem. Phys.* **2001**, *115*, 6426.

(33) Varetto, U. *Molekel 5.2.0.5*; Swiss National Supercomputing Centre: Manno, Switzerland. http://bioinformatics.org/molkel.

(34) Grossman, M. J.; Lee, M. K.; Prince, R. C.; Garrett, K. K.; George, G. N.; Pickering, I. J. *Appl. Environ. Microbiol.* **1999**, *65*, 181.

(35) Grossman, M. J.; Lee, M. K.; Prince, R. C.; Garrett, K. K.; George, G. N.; Pickering, I. J. *Appl. Environ. Microbiol.* **1999**, *65*, 3264.

(36) Kelemen, S. R.; George, G. N.; Gorbaty, M. L. *Fuel Process. Technol.* **1990**, *24*, 425.

(37) Dezarnaud-Dandine, C.; Bournel, F.; Mangeney, C.; Tronc, M.; Modelli, A.; Jones, D. *Chem. Phys.* **2001**, *265*, 105.

(38) Sarangi, R.; DeBeerGeorge, S.; Rudd, D. J.; Szilagyi, R. K.; Ribas, X.; Rovira, C.; Almeida, M.; Hodgson, K. O.; Hedman, B.; Solomon, E. I. *J. Am. Chem. Soc.* **2007**, *129*, 2316.

(39) Ankudinov, A. L.; Ravel, B.; Rehr, J. J.; Conradson, S. D. *Phys. Rev. B* **1998**, *58*, 7565.

(40) Rehr, J. J.; Albers, R. C. *Rev. Mod. Phys.* **2000**, *72*, 621.

(41) De Peinder, P.; Petrauskas, D. D.; Singelenberg, F.; Salvatori, F.; Visser, T.; Soulimani, F.; Weckhuysen, B. M. *Appl. Spectrosc.* **2008**, *62*, 414.

(42) De Peinder, P.; Visser, T.; Petrauskas, D. D.; Salvatori, F.; Soulimani, F.; Weckhuysen, B. M. *Energy Fuels* **2009**, *23*, 2164.

(43) de Peinder, P.; Visser, T.; Petrauskas, D. D.; Salvatori, F.; Soulimani, F.; Weckhuysen, B. M. *Vib. Spectrosc* **2009**, *51*, 205.